Supporting Information

Pontani et al. 10.1073/pnas.1201499109

SI Text

Theoretical Model for the Same Size Droplets. We present here the full expression of the energies used in our model. The droplets of equal initial radii R_o are pushed one against the other by an external load F. We assume that the droplet shape is spherical with a radius R except for a flat "interface." Distributions of radii will be considered in a second part. The system is parameterized by the distance h between the flat surfaces and the deformation angle θ. The free energy reference is taken for $h \to \infty$. We assume volume conservation leading to the following relation between R and R_o:

$$R = R_o\left[\frac{4}{4-(1-cos(\theta))^2(2+cos(\theta))}\right]^{1/3}.$$

The total free energy of the system is the sum of three terms:

1. **Electrostatic repulsion**. We assume a small deformation angle θ so that the repulsion between the droplets can be evaluated as the electrostatic repulsion of 2 charged spheres in the approximation of Derjaguin, and we write $E_e = 2\pi\epsilon\psi_o^2 R_o \exp^{(-\kappa h)}$ where ϵ is the dielectric constant, ψ_o is the electrical potential at the droplet surface, and κ the inverse of the Debye length. This is a reasonable fit of experimentally measured electrostatic repulsion between 2 charged colloidal particles in the case of a diffuse Debye layer.
2. **Deformation energy**.

$$E_d = 2\sigma\pi R[(\sin^2(\theta) + 2(1+\cos(\theta)) - 4]$$

where σ is the surface tension and the second term corresponds to the change in surface area.
3. **Binding energy**. We assume that binding occurs only for interdroplets distances h smaller than a critical distance h_c corresponding to the outreach of the biotin/streptavidin complex grafted on their PEG spacer. This distance is evaluated as $h_c = 18$ nm. The energy then writes

$$E_b = c_b\epsilon_b(R\sin(\theta))^2 H(h_c - h)$$

where c_p is the binder concentration in the patch and e_b is the binding energy of an individual binder (biotin/streptavidin). Neglecting the h dependence of the entropic term in the binding energy we model the interaction with the step Heaviside function $H(t)$.

We neglected the Van Der Waals interactions because they are largely reduced in our system due to the index matching of the water with the oil. The equilibrium position is given by the condition

$$\nabla_d(E_e + E_d + E_b) = -F$$

where $d = 2R\cos(\theta) + h$ is the distance between the droplet centers. It is equivalent to

$$\nabla_d(E_d + E_e + E_b + Fd) = 0.$$

$W_l = Fd$ can thus be considered as an effective potential energy. In the rest of the text we call $E = E_d + E_e + E_b + W_l$ and we minimize it with respect to h and θ to find the equilibrium positions. The minimum must be computed numerically although an analytic solution can be found for small angles. The total energy has thus a fourth order polynomial expression with a discontinuity at $h = h_c$. As shown in Fig. 2*B*, the energy landscape reveals two local minima in the (θ, h) plane for values $E_1 = E(\theta_1, h_1)$ and $E_2 = E(\theta_2, h_2)$ where

- $h_1 = \frac{1}{\kappa}\ln(\frac{2\pi\kappa\epsilon\psi_o^2 R_o}{F})$
- $\theta_1 = \begin{cases} \theta_{\text{unbound}} = (\frac{12FR_o}{5FR_o+12\pi R_o^2\sigma})^{1/2} & \text{if } h_1 > h_c \\ \theta_{\text{bound}} = (\frac{12(FR_o+e_b\pi R_o^2)}{5FR_o+8\cdot e_b\pi R_o^2+12\pi R_o^2\sigma})^{1/2} & \text{if } h_1 \le h_c \end{cases}$
- $\theta_2 = \theta_{\text{bound}}$

In the limit of small deformations ($\theta \ll 1$) E the total energy can be expanded to its fourth order term leading to

$$E = -A\theta^2 + B\theta^4 + C(h)$$

where

$$A = FR_o + c_p e_b \pi R_o^2 H(h_c - h)$$
$$B = \frac{1}{24}(5FR_o + 8c_p e_b \pi R_o^2 H(h_c - h) + 12\pi R_o^2\sigma)$$
$$C(h) = Fh + 2\pi\epsilon\psi_o^2 R_o \exp(-\kappa h).$$

Onset of Spontaneous Patch Formation. We calculate ΔE at $F = 0$. The limit case where adhesion occurs is for $\Delta E = 0$. In this limit the deformation are small enough to use the Taylor expansion of the energy.

$$\Delta E = \frac{F_c}{\kappa} - \frac{3e_b^2}{e_b + 3\pi Ro^2\sigma}$$

with $F_c = 2\pi\kappa\epsilon\psi_o^2 R_o \exp(-\kappa h_c)$ with a unique positive solution:

$$e_b^c = \frac{\alpha}{6\pi R_o^2} e^{-\kappa h_c}\left[1 + \left(1 + \frac{36\pi R_o^2\sigma}{\alpha} e^{\kappa h_c}\right)^{0.5}\right].$$

Increasing the salt or the binder concentration will set e_b above e_b^c enabling spontaneous adhesion to occur. The dependance of e_b^c with C and κ is plotted in Fig. 1.

Theoretical Model for Polydisperse Droplets. We now consider the case of unequal droplet radii. We call R_1 and R_2 the two radii of the deformed droplet. The common contact area sets $R_1\sin(\theta_1) = R_2\sin(\theta_2)$ and hence to the first relevant order $\theta_2 = \frac{R_1}{R_2}\theta_1$. The electrostatic repulsion now reads

$$E_e = \pi\epsilon\psi_o^2(R_1 + R_2)\exp^{-\kappa h}.$$

The deformation energy:

$$E_d = \sigma\pi R_1[\sin^2(\theta_1) + 2(1+\cos(\theta_1)) - 4] + \sigma\pi R_2[\sin^2(\theta_2) + 2(1+\cos(\theta_2)) - 4]. \quad \textbf{[S1]}$$

The binding energy is unchanged. The final expression for the total energy is

$$E = -A\theta^2 + B\theta^4 + C(h)$$

where

$$A = \frac{FR_1}{2} + \frac{FR_1^2}{2R_2} + e_b \pi R_1^2 H(h_c - h)$$

$$B = \frac{5FR_1}{48} + \frac{FR_1^2}{R_2} + \frac{1}{3} e_b \pi R_1^2 H(h_c - h) - \frac{FR_1^4}{16R_2^2} + \frac{\pi}{4} R_1^2 \sigma + \frac{\pi R_1^4 \sigma}{4R_2^2}$$

$$C(h) = Fh + \pi \epsilon \psi_o^2 (R_1 + R_2) \exp(-\kappa h).$$

The phase diagram for a polydisperse emulsion is constructed as follows. The distribution of radii of contacting droplet is extracted from the experimental results. We calculate the phase diagram for given pair of R_1 and R_2. The final phase diagram is the average of individual pair diagram weighted by the pair experimental occurrence.

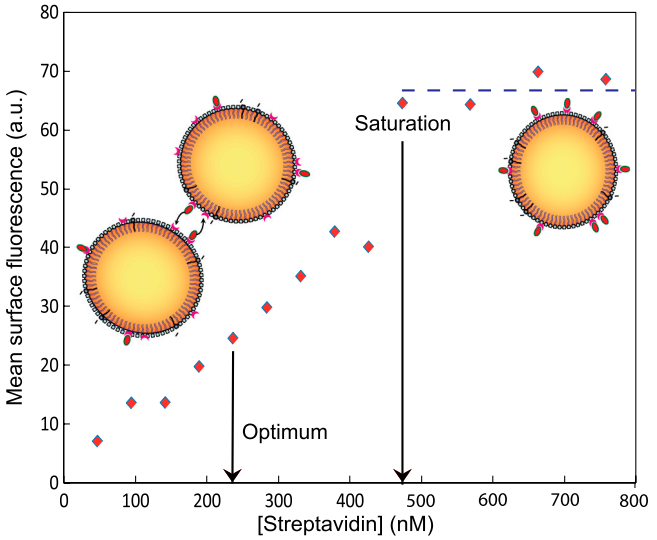

Fig. S1. Texas red streptavidin is introduced in the continuous phase to label the biotinylated lipids present on the droplet surfaces. The average fluorescence intensity is measured on the droplets for streptavidin concentrations ranging from 47 up to 758 nM solution after 1 hr of incubation at room temperature. When all the biotinylated lipids on the surface are bound to streptavidin, the fluorescence on the surface saturates, as shown by the plateau at $[\text{streptavidin}]_{\text{saturation}} = 473$ nM. The optimal concentration point for binding two biotins on contacting droplets through one streptavidin is reached when half the biotins on each surface are decorated with streptavidins, as shown in the schematic. We therefore use half of the saturation concentration of streptavidin throughout this study. If all the streptavidins were on the droplet surfaces and not in the bulk, the fluorescence measurements would give an upper bound of $1.4 * 103$ binders/μm^2 on the surface. Because streptavidin is readily soluble in the aqueous phase the binder concentration is more accurately estimated by our model in the manuscript to be an order of magnitude lower than this upper bound. The concentration of biotinylated lipids on the surface is set by the competition between the lipids and SDS molecules to stabilize the interface. For example, raising the SDS concentration from 1 to 5 mM causes on average a 2.5-fold decrease in the surface fluorescence from the lipid-bound streptavidin, in agreement with a decrease in the binder concentration predicted by the model.

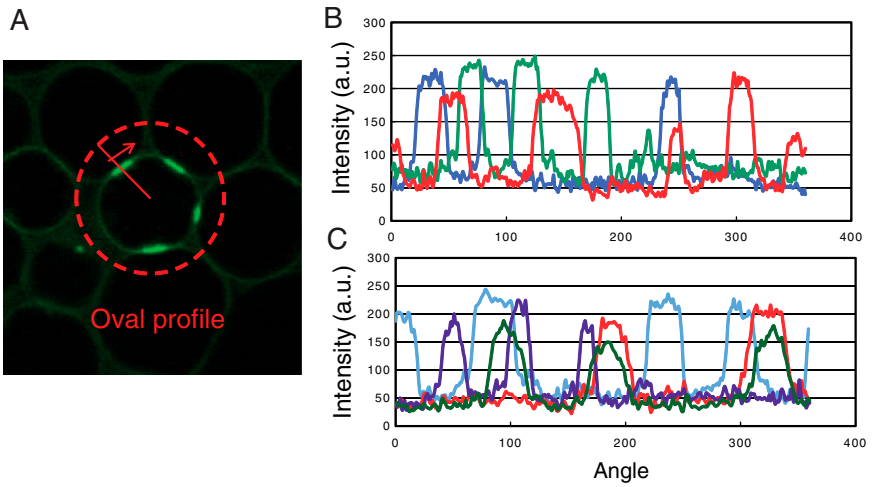

Fig. S2. (*A*) Streptavidin fluorescence around the droplets is analyzed in 2D confocal images. The surface intensity values are identified using the plugin "Oval Profile Plot" in ImageJ. This plugin outputs the maximum intensity value along the radius taken from the center of the droplet to a circle around it (red circle). The measure is repeated 360 times by rotating the radius and the resulting profiles are shown in *B* for 7 droplets randomly picked in different emulsions. The higher plateau values correspond to the enhanced regions of the patches and are several times higher than the value at the perimeter. This indicates that these regions correspond to an enrichment of the streptavidin at the deformation sites where the patches appear. Therefore we qualify those regions of enhanced intensity as adhesion patches.

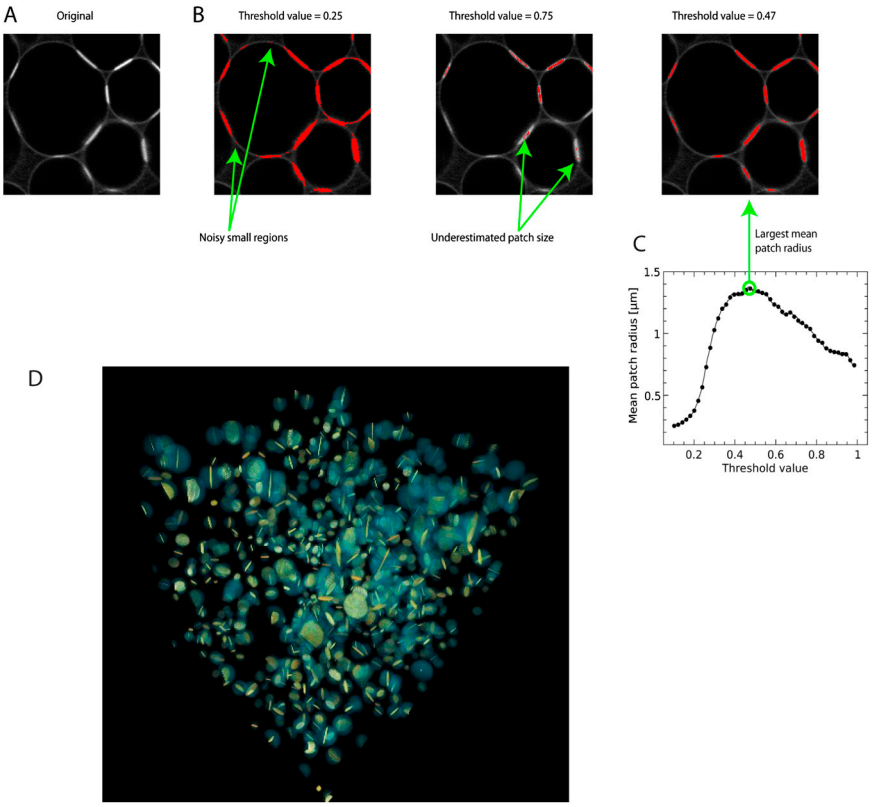

Fig. S3. (*A*) Patches formed by protein bonds are revealed by enhanced fluorescence on the droplet surfaces as shown in these 2D confocal images. (*B*) The images acquired through confocal microscopy are thresholded such that only the pixels that are bright enough belong to a patch. (*C*) The optimal threshold value is chosen to be that at which the largest mean patch size is reached. (*D*) To identify the discs corresponding to patches we draw the smallest sphere centered at the center of mass of the patch that contains the whole patch. The radius of the patch r_p is given by the radius of the corresponding sphere.

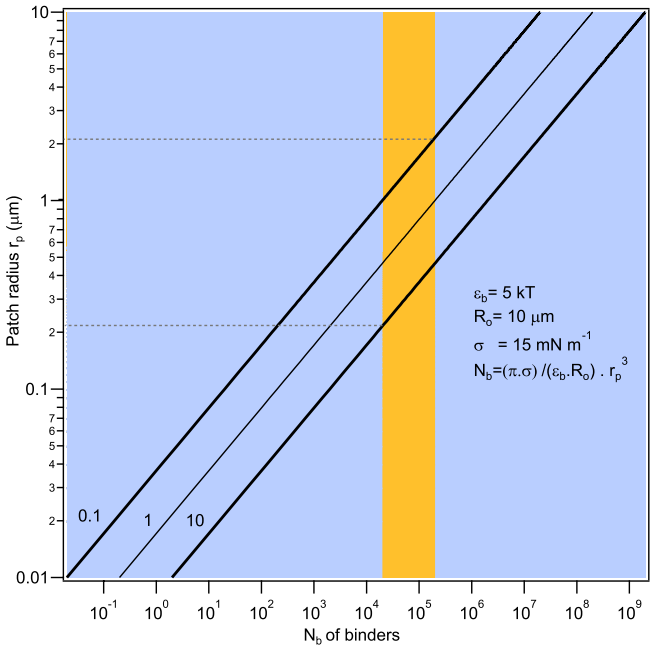

Fig. S4. Minimal patch size with no applied force as a function of the number of binding proteins on the surface. This patch size is estimated for physiological salt concentrations of 100 mM NaCl and the adhesion energy corresponding to e-cadherin homophilic binding of ≈5 kT. The yellow zone corresponds to the estimate of the total number of cadherins on a cell surface. The line labeled as 1 is calculated with the values indicated on the graph and shifted to the other lines with an additional prefactor 10 (line 10) or 0.1 (line 0.1) to account for variations in the estimates of ϵ_b and σ. This graph shows that small patches will be induced even in the absence of force between cells, but the size of those patches (known as puncta) is insufficient for the mechanical integrity of cells in tissue.

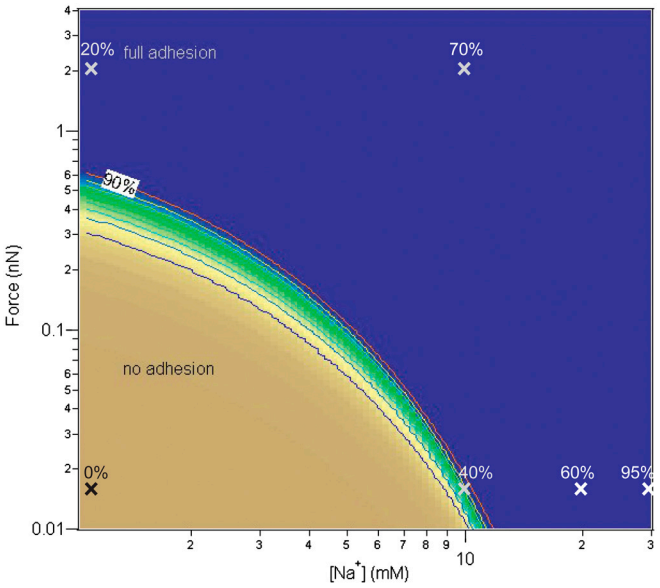

Fig. S5. Phase diagram for adhesion in the 1 mM SDS emulsion. The following parameters: $\sigma = 15$ m Nm^{-1};$\epsilon_b = 15$ kT; $\zeta = -50$ mV; $c_b = 6 * 10^{13}$ molecules/m^2 were found as best fitting parameters for the predicted phase diagram with our experimental data. The theoretical 90% patch fraction line is plotted as labeled and the experimental points are superimposed on the phase diagram for various conditions.

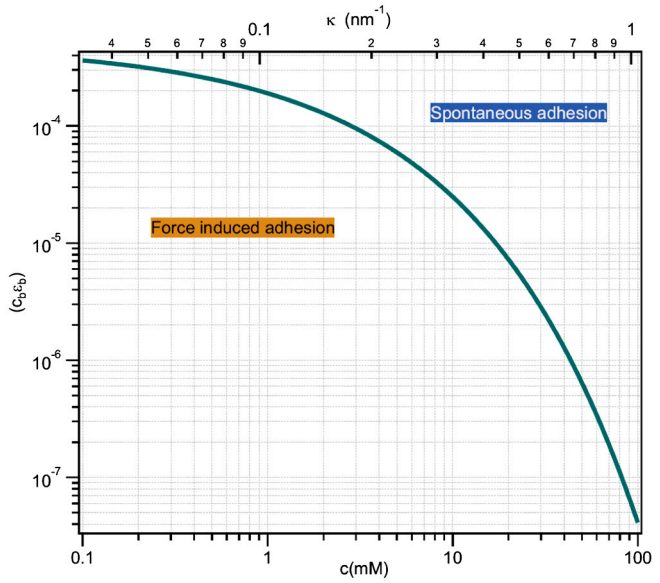

Fig. S6. Critical values of $c_b \cdot \epsilon_b$ for spontaneous adhesion as a function of the salt concentration (bottom) or inverse Debye Length (top). It can also be seen as the phase diagram of adhesion at zero force as a function of salt and binder concentration.

Table S1. Principal characteristics of the emulsion conditions used in the experiments are compared with the same cellular parameters

	1 mM SDS2 mM Tris-HCl	5 mM SDS2 mM Tris-HCl	Cells
Zeta potential *mV*	−29.9 ± 11.1	−71.8 ± 14.8	[−32; −15] (1, 2)
Surface tension $mN \cdot m^{-1}$	15 (3)	12.5 (4)	[1; 15] (5–7)
$[\text{streptavidin}]_{surface}$ $molecules \cdot m^{-2}$	$6 * 10^{13}$	$4.7 * 10^{13}$	$[8 * 10^{13}; 8 * 10^{14}]$ (5, 8)
Binding energy ε_b *kT*	15 (9)	15 (9)	9–11 (10)

The zeta potential was measured on our emulsions using a Zetasizer Nano ZS (Malvern Instruments). The cellular zeta potential was measured for different cell lines in the literature for epithelial cell line MCF10A and for the MCF7 cancer cells (1, 2). Surface tension measurements were previously reported in the literature for emulsions stabilized with the same SDS concentrations (3, 4). Cell surface tension is obtained from measurements on cellular aggregates in (5–7). The surface concentrations of proteins are derived from the model fits in Fig. 5 in the manuscript and compared with the values for cadherins in cells (5, 8). The binding energy measured in (9) is used to fit the phase diagram, while the binding energy between cadherins is estimated in ref. 10.

1 Zhang Y, et al. (2008) Zeta potential: a surface electrical characteristic to probe the interaction of nanoparticles with normal and cancer human breast epithelial cells. *Biomed Microdevices* 10:321–328.
2 Fontes A, et al. (2011) Mechanical and electrical properties of red blood cells using optical tweezers. *Journal of Optics* 13:044012.
3 Neumann B, et al. (2004) Stability of various silicone oil/water emulsion films as a function of surfactant and salt concentration. *Langmuir* 20:4336–4344.
4 Umbanhowar PB, et al. (2000) Monodisperse emulsion generation via drop break off in a coflowing stream. *Langmuir* 16:347–351.
5 Foty RA, Steinberg MS (2005) The differential adhesion hypothesis: a direct evaluation. *Developmental Biology* 278:255–263.
6 Manning ML, et al. (2010) Coaction of intercellular adhesion and cortical tension specifies tissue surface tension. *Proc Nat'l Acad Sci USA* 107:12517–12522.
7 Guevorkian K, et al. (2010) Aspiration of biological viscoelastic drops. *Phys Rev Lett* 104:218101.
8 Chen CP, et al. (2005) Specificity of cell-cell adhesion by classical cadherins: Critical role for low-affinity dimerization through beta-strand swapping. *Proc Nat'l Acad Sci USA* 102:8531–8536.
9 Walker SA, et al. (1995) Controlled multi-stage self assembly of vesicles. *MRS Proceedings* 372:95–100.
10 Katsamba P, et al. (2009) Linking molecular affinity and cellular specificity in cadherin-mediated adhesion. *Proc Nat'l Acad Sci USA* 106:11594–11599.